

Mass-velocity correlation in impact induced fragmentation of heterogeneous solids

Gergő Pál¹ · Ferenc Kun¹ 

Received: 9 March 2016
© Springer-Verlag Berlin Heidelberg 2016

Abstract We study the impact fragmentation of disordered solids by means of a discrete element model focusing on the velocity and mass-velocity correlation of fragments. Simulations are performed with plate-like objects varying the plate thickness and the impact velocity in broad ranges. Depending on the impact velocity the breakup process has two different outcomes: at low velocities the sample gets only damaged, to achieve fragmentation, where no large residues survive, the impact velocity has to surpass a critical value. In the fragmented phase the velocity components of fragments are power law distributed with a stretched exponential cutoff, where the impact velocity and plate thickness mainly control the standard deviation of the distributions. Mass velocity correlation is only pointed out for thin plates, while it disappears for three-dimensional bulk samples. In the damage phase of thin plates the mass and velocity of fragments proved to be strongly correlated, however, in the fragmented phase correlation occurs in the vicinity of the critical velocity and it is limited to the large fragments only. The correlation function decays as a power law with different exponents for small and large fragments in good agreement with recent experimental findings. We show that the mass-velocity correlation originates from the spatial dependence of the mass and velocity of pieces inside the fragmenting body.

Keywords Impact fragmentation · DEM · Velocity distribution · Mass-velocity correlation

1 Introduction

Energetic loading of solid bodies such as explosion, collision, or impact leads to sudden disintegration into a large number of pieces [1,2]. Such fragmentation processes are abundant in nature, from the collapse of rock walls through the pyroclastic activity of volcanic eruptions to the breakup of glaciers [3] several geological examples can be mentioned [4]. In particular, the impact induced fragmentation of solids plays a crucial role in the evolution of asteroids in the Solar system: during their history asteroids have undergone a large number of collisions with different energies ranging from crater creation to a high degree of shattering [5]. Breakup processes are also exploited by the industry, i.e. the controlled fragmentation of heterogeneous brittle materials has a high importance in mining and ore processing where a certain degree of size reduction has to be achieved with moderate energy costs [2,4].

During the past decades research on fragmentation mainly focused on the statistics of fragment sizes/masses which revealed that these quantities are power law distributed with universal exponents [6–15]. Recently, it has been pointed out that the shape of fragments obeys also scaling laws with a high degree of robustness [16–18]. However, it often occurs that to infer the consequences of fragmentation events, more detailed information is needed about the fragments going beyond the description of their size, mass, and shape. For instance, the time evolution of fragment clouds after asteroid impacts can only be determined based on the velocity of the created pieces [5]. Similar problem occurs at the sudden collapse of rock walls or landslide triggered rock avalanches [19,20] where knowledge on the velocity of fragments is essential to quantify the secondary fragmentation of pieces and to estimate the run-out distance and destruction power of the avalanche [19,20].

✉ Ferenc Kun
ferenc.kun@science.unideb.hu

¹ Department of Theoretical Physics, University of Debrecen, Debrecen P.O. Box 5, 4010, Hungary

A large number of laboratory experiments have been performed on various types of heterogeneous materials using high speed imaging techniques to determine the speed of fragments [21–24]. Some experiments revealed a power law correlation of the mass and velocity of fragments, i.e. the average velocity of fragments was found to decrease as a power of their mass [21–23]. However, other studies found weak or even no correlation [24, 25] and pointed out the problem of incomplete experimental information caused by the missing fragments, not captured by imaging, which bias the results [25].

In the present paper we study the impact fragmentation of disordered solids based on a three-dimensional discrete element model with the aim to analyze the velocity distribution and the correlation of the mass and velocity of fragments. Realistic simulations allow us to overcome the limitations of experiments providing access to all details of the fragmenting system. In order to understand how the geometry of the sample affects the velocity of the generated fragments, simulations were carried out for the breakup of plate-like solids embedded in the three-dimensional space varying the thickness of the sample from quasi two-dimensional thin plates to three-dimensional bulk. Analyzing the spatial arrangement of fragments we could also get an insight into the origin of the mass-velocity correlation of fragments. Our results provide a possible explanation for recent experimental findings on the fragmentation of heterogeneous brittle materials.

2 Discrete element simulation of impact fragmentation

Recently, we have worked out a discrete element model of heterogeneous materials in three dimensions [26, 27]. The model has been successfully applied to investigate the compressive failure of sedimentary rocks [26, 27] and fragmentation processes due to impact [15]. Here we briefly review the main ingredients of the model construction focusing on the specific features relevant for the present study.

In the model the sample is represented as a random packing of spherical particles with a uniform distribution of the diameter d in a narrow interval Δd around the average $\langle d \rangle$ with $\Delta d / \langle d \rangle = 0.05$ [15]. Cohesive interaction is provided by beams which connect the particles along the edges of a Delaunay triangulation of the initial particle positions. In three dimensions (3D) the total deformation of a beam is calculated as the superposition of elongation, torsion, as well as, bending and shearing [28]. Cracks are formed when overstressed beams break according to a physical breaking rule. The breaking condition takes into account the stretching and bending of beams [29–31]

$$\left(\frac{\varepsilon_{ij}}{\varepsilon_{th}} \right)^2 + \frac{\max(\Theta_i, \Theta_j)}{\Theta_{th}} \geq 1, \quad (1)$$

where the two parameters ε_{th} and Θ_{th} control the relative importance of the corresponding breaking modes. In Eq. (1) ε_{ij} denotes the axial strain, while Θ_i , and Θ_j are the bending angles of the beam ends between particles i and j . The interaction of contacting particles which are not connected by beams is described by the Hertz contact law [28]. In the model there is only structural disorder present: the breaking thresholds ε_{th} and Θ_{th} are constants, however, the physical properties of beams are determined by the random particle packing. The energy stored in a beam just before breaking is released in the breakage giving rise to energy dissipation. At the broken beams along the surface of the spheres cracks are generated inside the solid and as a result of the successive beam breaking the solid falls apart. The time evolution of the fragmenting solid is obtained by solving the equations of motion of the individual particles until the entire system relaxes meaning that no beam breaking occurs during some hundreds of consecutive time steps and there is no energy stored in deformation.

In the present study we use the model to investigate the impact induced breakup of plate-like bodies. The overall layout of the samples is the same as in Ref. [15]: plate-like samples were constructed with a rectangular basis of side length L and height H . All simulations were carried out with the linear extensions $L = 30$ varying the sample height in the range $H = 3–15$ measured in units of the average particle diameter $\langle d \rangle$. For the microscopic parameters of the model, i.e. for the elastic parameters of the particles, beam element the same values were used as in Refs. [15, 26, 27], which represent a random heterogeneous material with quasi-brittle macroscopic response.

Impact loading was realized in such a way that a single surface particle was selected in the middle of one of the side walls of the sample, which together with its contacting neighbors got an initial velocity v_0 pointing towards the center of mass of the body. This loading condition provides a good representation of impact loading where a stopper prevents the penetration of the impactor into the target [24, 32, 33], or the explosion of a contact charge is applied to generate a stress pulse on the surface of the sample [34]. In the present study a large number of simulations were carried out varying the impact velocity v_0 in a broad range from damaging the sample around the impact point to a high degree of shattering.

Fragments are identified in the final state of the time evolution as clusters of particles connected by the surviving beam elements. To characterize individual fragments we determined their mass m_i and velocity vector \mathbf{v}_i in the final state, furthermore, their position \mathbf{r}_i^0 in the initial state inside the original body. The mass of a fragment is simply obtained as the sum of the mass m_j^p of its particles of index j

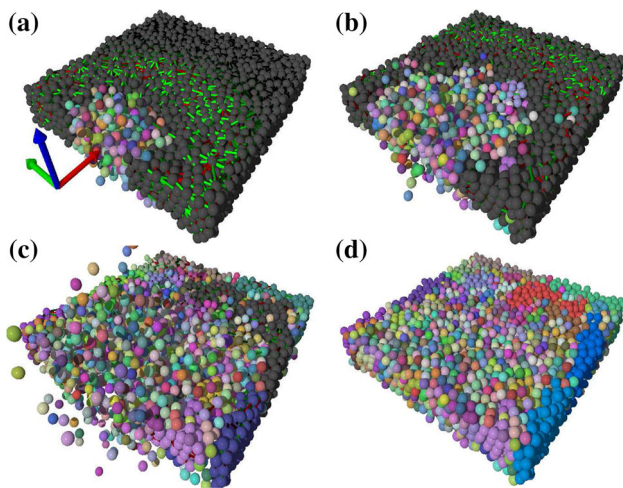


Fig. 1 (Color online) Time evolution of the fragmentation process of a plate of thickness $H = 5$. Beams are colored according to their deformation so that the elastic wave is visible in (a) then the solid gradually breaks up in (b) and (c). Particles of different fragments have randomly selected colors. In (d) the body is reassembled to have a better view on the spatial arrangement of fragments and on the structure of cracks. The coordinate system used in the calculations is illustrated in (a) where the x (red), y (green), and z axes are aligned with the impact velocity and with the edges of the body, while the origin is fixed to the impact site

$$m_i = \sum_{j=1}^{n_i} m_j^p, \tag{2}$$

where n_i denotes the number particles of fragment i . The center of mass position \mathbf{r}_i^0 and velocity \mathbf{v}_i of fragments are calculated as

$$\mathbf{r}_i^0 = \frac{\sum_{j=1}^{n_i} m_j^p \mathbf{r}_j^{p0}}{m_i}, \tag{3}$$

$$\mathbf{v}_i = \frac{\sum_{j=1}^{n_i} m_j^p \mathbf{v}_j^p}{m_i}, \tag{4}$$

where \mathbf{r}_j^{p0} and \mathbf{v}_j^p are the position of particle j in the initial state and its velocity in the final state of the process, respectively.

A representative example of the impact induced breakup of a sample of $H = 5$ is shown in Fig. 1 for an impact velocity where a high degree of shattering is achieved. In Fig. 1d the final reassembled sample is presented where all particles are put back to their position inside the original body where the fragment positions \mathbf{r}_i^0 are determined. This representation of the data facilitates to observe the spatial structure of cracks. We carried out simulations to determine the speed c of the compression wave of the model material so that in the following the velocity values will be presented in a dimensionless form utilizing the value of c .

3 Damage and fragmentation

When studying the velocity distribution of fragments the degree of breakup is crucial, hence, here we briefly summarize the most important findings on this subject relevant for the present study. It has been pointed out for the dynamic breakup of solids that increasing the imparted energy the system undergoes a phase transition [35]: at low values of the imparted energy the solid body suffers only damage, i.e. mainly small sized fragments are created together with a large residue comparable to the original body. To achieve breakup the imparted energy has to surpass a critical value above which even the largest fragment gets significantly smaller than the initial sample. This damage–fragmentation transition has been found under various types of loading conditions from projectile impact, through explosion generated breakup to the collision of macroscopic bodies [36–38]. The transition occurs at a well defined critical point showing strong analogy to continuous phase transitions [10, 13, 14, 31, 35].

Recently, we have demonstrated the damage–fragmentation transition for the impact induced breakup of plate like objects [15] studied also in the present paper. Analyzing the behavior of the average mass of fragments as a function of the impact velocity v_0 , we determined the critical value v_c of v_0 at which fragmentation first occurs. Simulations revealed that v_c increases as a power law of the plate thickness

$$v_c \sim H^\alpha, \tag{5}$$

where the exponent was obtained as $\alpha = 0.2$ [15]. The precise value of the critical impact velocity falls in the range $v_c/c = 0.19\text{--}0.23$ as H increases from 3 to 15 [15].

In the fragmented phase $v_0 > v_c$ the mass distribution of fragments proved to be a power law

$$p(m) \sim m^{-\tau} \tag{6}$$

in agreement with experimental findings. However, the value of the exponent τ is not universal in the sense that for low plate thickness the value of τ proved to increase from $\tau = 1.7$ to $\tau = 2.4$ above the critical point as the impact velocity increases. For three-dimensional bulk solids realized in our model at high plate thicknesses, a unique exponent $\tau = 2.4$ is obtained [15]. Our computer simulations revealed that an underlying transition in the structure of the crack pattern responsible for the observed non-universality. For thin plates embedded into the 3D space the crack pattern of the fragmented phase of breakup has essentially two types: when the impact velocity v_0 falls close to the critical point the interference pattern of elastic waves generates a two dimensional crack pattern which has a high degree of regularity. At higher impact velocities cracking in the bulk of the plate gets acti-

vated which leads to a disordered three dimensional pattern. The regular two-dimensional crack pattern and the disordered three-dimensional one favor a lower and a higher value of the mass distribution exponent. The gradual transition between the two limits is controlled by the impact velocity in the fragmented phase. For more details see Ref. [15].

In the present paper we investigate the velocity distribution of fragments, furthermore, the relation between the velocity, spatial position and mass of fragments both in the damage and fragmented phases at different plate thicknesses. The thickness dependent critical velocity of damage-fragmentation transition will be utilized from Ref. [15].

4 Velocity distribution of fragments

The center of mass velocity of fragments is determined in the final state of the fragmentation process where the cloud of fragments is expanding without further breaking. The coordinate system used in the calculations is illustrated in Fig. 1 where the x axis is aligned with the impact velocity. Due to momentum conservation the system has symmetry with respect to the y and z axes of the coordinate system.

The probability distribution $p(v_y)$ of the y component of the fragment velocity v_y is presented in Fig. 2a at the smallest plate thickness considered $H = 3$ for several values of the impact velocity v_0 in the fragmented regime $v_0 > v_c$. All distributions are peaked at $v_y = 0$ and are symmetric func-

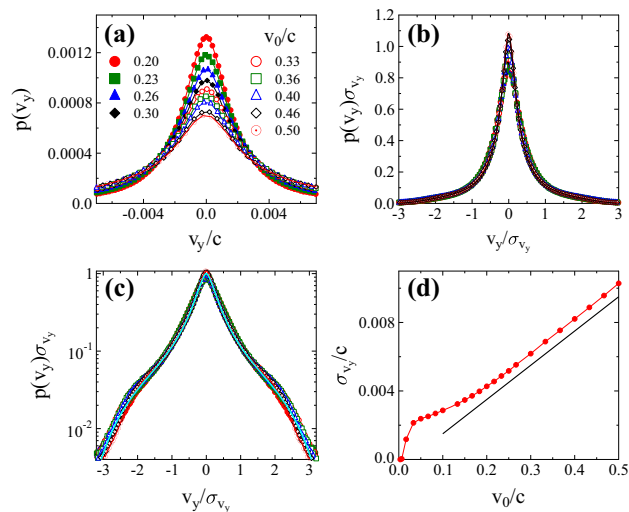


Fig. 2 (Color online) **a** Probability distribution $p(v_y)$ of the velocity component v_y for the lowest plate thickness $H = 3$ at several values of the impact velocity v_0 in the fragmented phase $v_0 > v_c$ of the system, where $v_c/c = 0.19$. **b** Rescaling the two axes with the standard deviation σ_{v_y} good quality data collapse is obtained. **c** The data collapse is shown on a semi-log plot. The *bold line* represents the best fit obtained with the functional form Eq. (8). **d** The standard deviation as a function of v_0 . The *straight line* is drawn to guide the eye

tions about the zero average $\langle v_y \rangle = 0$ as it is expected. As the impact velocity v_0 increases the functional form of $p(v_y)$ remains the same, however, the distributions get broader. In order to quantify the increasing scatter of the velocity component v_y , we calculated the standard deviation σ_{v_y} of the distributions as $\sigma_{v_y} = \sqrt{\langle v_y^2 \rangle - \langle v_y \rangle^2}$. It can be observed in Fig. 2b that rescaling the distributions $p(v_y, v_0)$ with the corresponding value of the standard deviation σ_{v_y} all the curves corresponding to different impact velocities v_0 can be well collapsed on a master curve. The quality of collapse is better seen in Fig. 2c where semi-log representation is used. The good quality data collapse implies that the distributions $p(v_y, v_0)$ depend on the impact velocity through the standard deviation in the form

$$p(v_y, v_0) = \sigma_{v_y}^{-1} \Phi(v_y/\sigma_{v_y}), \quad (7)$$

where $\Phi(\lambda)$ denotes the scaling function. The velocity v_0 dependence of σ_{v_y} is illustrated in Fig. 2d for the entire range of impact velocities including also the damage phase of the system. In the fragmented regime σ_{v_y} is found to increase linearly with the impact velocity $\sigma_{v_y} \sim v_0$, while in the damage phase a more rapid increase is evidenced.

The master curve in Fig. 2c obtained by the scaling analysis can be well fitted with the functional form

$$\Phi(\lambda) = A \frac{1}{B + \lambda^\mu} \exp(-(\lambda/\lambda^*)^\beta), \quad (8)$$

which is a power law of exponent μ for intermediate values of the scaling variable $\lambda = v_y/\sigma_{v_y}$, followed by a stretched exponential cutoff. The additive parameter B regularizes the shape of the distribution in the vicinity of $\lambda = 0$, while the exponent β controls the shape of the cutoff. It can be observed in Fig. 2c that Eq. (8) provides a good description of the numerical data, best fit is obtained with the parameter values $\mu = 1.7$, $\beta = 3.1$, $A = 0.12$, $B = 0.1$, and $\lambda^* = 2.15$.

The distribution $p(v_z, v_0)$ of the z component of the fragment velocity has a similar behavior (see Fig. 3), i.e. a symmetric functional form is obtained peaked at zero velocity. Varying the impact velocity v_0 the distributions $p(v_z, v_0)$ change in the same qualitative way and obey the same scaling structure as $p(v_y, v_0)$ (see Fig. 3c).

Increasing the plate thickness essentially the same qualitative behavior is obtained for $p(v_y, v_0)$ and $p(v_z, v_0)$ as we have seen above for $H = 3$, however, the thickness affects the standard deviations σ_{v_y} and σ_{v_z} . As an example, the inset of Fig. 4 presents the velocity dependence v_0 of the standard deviation σ_{v_y} for each thickness H considered. It is interesting to note that in the fragmented phase of the system σ_{v_y} linearly increases with the impact velocity v_0 , and it decreases with increasing plate thickness H . The

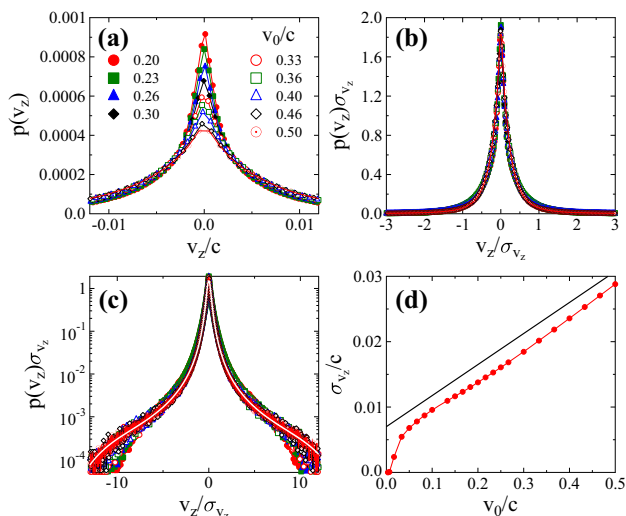


Fig. 3 (Color online) **a** Probability distribution $p(v_z)$ of the velocity component v_z for the plate thickness $H = 3$ at several values of the impact velocity v_0 in the fragmented phase. **b** Good quality data collapse is obtained by rescaling the two axes with the standard deviation σ_{v_z} of the velocities. **c** The functional form of Eq. (8) well describes the master curve. **d** The standard deviation linearly increases with v_0 in the fragmented phase

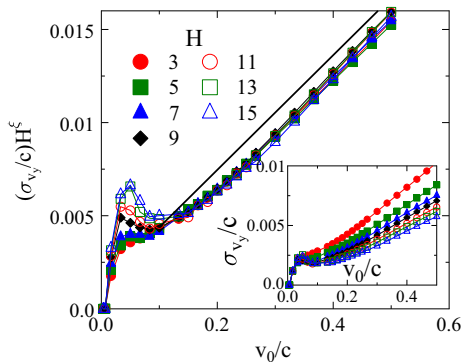


Fig. 4 (Color online) *Inset* standard deviation σ_{v_y} of the velocity component v_y of fragments as a function of the impact velocity v_0 for all thicknesses H considered. *Main panel* rescaling σ_{v_y} with a power ξ of H good quality data collapse is obtained

main panel of the figure demonstrates that the standard deviations obtained at different thicknesses H can be collapsed by rescaling along the vertical axis with an appropriate power of H . The good quality collapse implies the functional form

$$\sigma_{v_y}(v_0, H) \sim \frac{v_0}{H^\xi}, \tag{9}$$

in the fragmentation regime, where the exponent giving best collapse in Fig. 4 is $\xi = 0.36$. The data analysis revealed the same behavior for the standard deviation σ_{v_z} of v_z , however, with a higher value of the exponent $\xi = 0.5$ implying a stronger dependence on the plate thickness H . The higher exponent ξ is caused by the fact that the z axis is directed

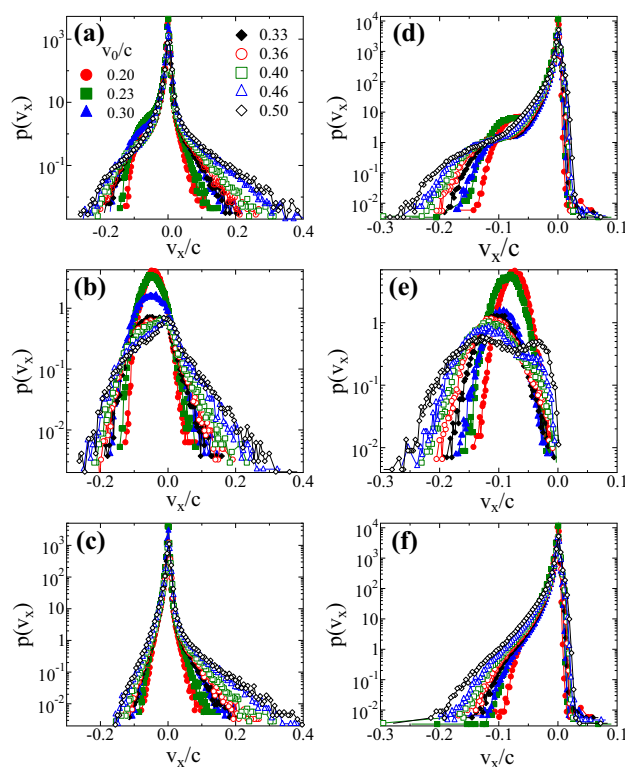


Fig. 5 (Color online) Probability distribution of v_x for the lowest $H = 3$ and highest $H = 15$ plate thicknesses presented in the *left and right columns*, respectively. **a, d** shows the complete distributions, **b, e** the distribution of the primary ejecta, while **c, f** present the distributions for the complementary data set

along the changing linear extension of the sample, while along the y direction the extension of the system is fixed and it has a greater value than in the y direction.

The distribution of the x component v_x of fragment velocities has a more complex behavior. Figure 5a, d presents $p(v_x, v_0)$ for the lowest and highest plate thicknesses $H = 3$ and $H = 15$, respectively. In both cases the same qualitative behavior can be observed, i.e. the distributions are asymmetric with a non-zero average value which increases with the impact velocity v_0 . Note that the positive x direction is aligned with v_0 pointing into the sample. Hence, fragments with negative values of v_x are back-scattered, while the ones with positive v_x move forward along the impact direction. Due to the conservation of linear momentum only a small fraction of the total mass of the body is comprised in the back-scattered fragments so that they are mainly single particles, i.e. powder in the model (see also Fig. 1). The source of the asymmetric form of the distributions $p(v_x)$ is that large mass fragments move forward $v_x > 0$, however, they have a significantly lower number than the back-scattered powder particles although they comprise the major fraction of the entire mass.

An interesting feature of the distributions is that for back-scattered fragments $v_x < 0$ a hump emerges, which implies

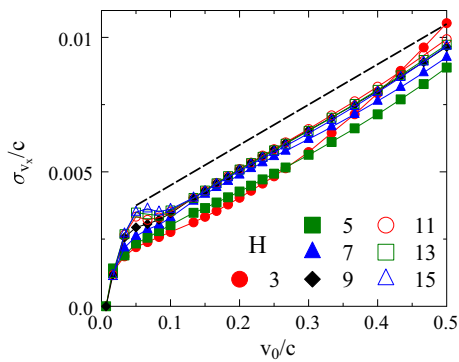


Fig. 6 (Color online) Standard deviation σ_{v_x} of v_x as a function of the impact velocity for all thicknesses considered. Except for the smallest thickness $H = 3$ the *straight line* gives a good approximation of the data in the fragmented phase

the emergence of a characteristic value of v_x . The hump gets less pronounced with increasing impact velocity. Careful sorting of the fragments according to their spatial position revealed that the hump is formed by back-scattered fragments which originate from a small volume about the impact site. These are those fragments which are ejected immediately after the initial impact without further interaction with the rest of the system. The velocity distribution of this primary ejecta is presented separately in Fig. 5b, e where a nearly Gaussian shape is obtained at lower impact velocities v_0 which then broadens as v_0 increases. The corresponding distribution of the complementary set, including all fragments except for the primary ejecta, is shown in Fig. 5c, f, where the functional forms are consistent with the distributions of v_y and v_z except for the asymmetry.

Increasing v_0 the distributions get broader so that the standard deviation σ_{v_x} increases linearly with the impact velocity $\sigma_{v_x} \sim v_0$ except for the smallest thickness $H = 3$, as it is illustrated in Fig. 6. Note that the value of σ_{v_x} only slightly changes with increasing thickness, above $H = 5$ it is practically constant.

5 Spatial dependence of fragments

To better understand the dynamics of the breakup process and how the velocity and mass of fragments are determined, it is instructive to analyze the spatial dependence of fragment properties. Since in the damage phase the number of fragments is rather limited, here we focus on the fragmented phase only.

5.1 Spatial dependence of fragment masses

We have shown earlier that for thin plates close to the critical point of fragmentation essentially a two-dimensional crack

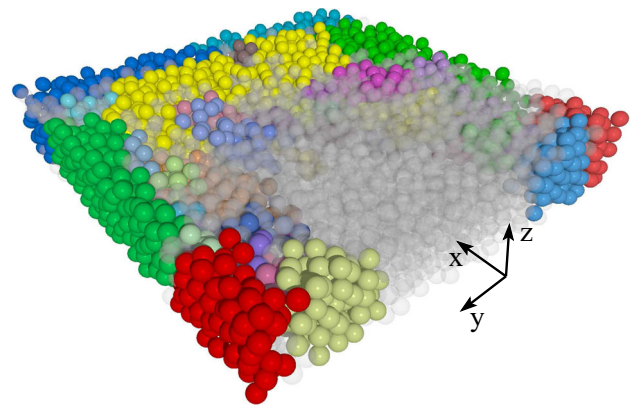


Fig. 7 (Color online) Fragments in a reassembled sample of thickness $H = 5$ at an impact velocity slightly above the critical point. The major fragments are highlighted with randomly assigned colors while the powder particles are made translucent gray. Except for the destructive zone around the impact point, the regular crack pattern can be inferred

structure emerges which is determined by the interference pattern of elastic waves generated by the impact loading [15]. In order to obtain quantitative information on how this crack pattern determines the spatial extension and mass of fragments, we determined the average mass of fragments as a function of their center of mass position inside the original body. For this purpose particles of the fragments were placed back to their original position inside the initial sample and then the center of mass coordinates (x_0, y_0) of fragments were determined using Eq. (3). Then both coordinates x_0 and y_0 were binned and the average mass $\langle m \rangle$ of fragments with coordinates falling in a bin was calculated. As a representative example Fig. 7 presents the final reassembled configuration of a fragmented plate where the individual fragments are colored. The regularity of the crack pattern can easily be inferred by the naked eye.

Figure 8 presents the average fragment mass $\langle m \rangle$ in a thin plate $H = 3$ as function of the y_0 coordinate for several impact velocities in the fragmented phase of the system. It can be observed that for all impact velocities the curves have distinct maxima and minima which is caused by the regularity of the crack pattern. The minima of $\langle m \rangle$ correspond to spatial regions where mainly small sized fragments occurred, i.e. where powder (single particles) or small fragments are created by the abrasion of the surface of big fragments due to their relative velocity. However, the maxima of the curves indicate those regions where no extensive cracking occurs. Note that the vertical axis is rescaled with a power γ of the impact velocity v_0 resulting in a good quality data collapse except for the lowest impact velocity. The data collapse implies that the average mass of fragments at a given location y_0 has the scaling structure

$$\langle m \rangle (y_0/L, v_0) = v_0^{-\gamma} \Phi(y_0/L). \quad (10)$$

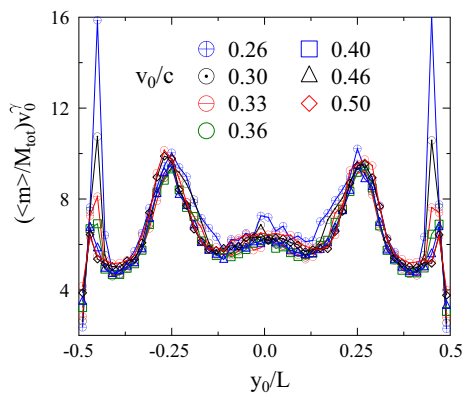


Fig. 8 (Color online) Average mass of fragments as a function of the y_0 coordinate of their center of mass position in the original body for the plate thickness $H = 3$. Along the vertical axis the data is rescaled with the impact velocity v_0 which results in a good quality collapse of the curves

The value of the scaling exponent γ providing best collapse is $\gamma = 0.8$. The sharp maximum of the curves close to the edges of the sample at $y_0/L \approx \pm 0.45$ are generated by the fragments of the detached boundary layers. The position of the detached zone practically does not change with the impact velocity because it is determined by the wave length of the compression wave in the body. The height of the detachment peaks in Fig. 8 decrease with v_0 because the detached layers break up into smaller and smaller fragments.

Considering the position dependence of the average fragment mass along the direction of impact, again local maxima and minima can be observed in Fig. 9, however, the curves do not show such a regular pattern what has been observed for the y_0 dependence. In the vicinity of the impact point the sample is completely shattered into powder (single particles) except for the detached boundary layers perpendicular to the impact direction. The detached corner pieces which are significantly larger than the surrounding powder particles are responsible for the small hump close to the sample surface at $x_0/L \approx 0.1$. Along the impact direction the average fragment mass increases until it reaches a maximum at $x_0/L \approx 0.6-0.8$ where the majority of the large fragments are located (see also Fig. 7). This maximum gets gradually shifted towards the edge of the sample with increasing v_0 since the shattered zone at the impact site spans deeper into the sample. The strong peak at $x_0/L \approx 0.92$ opposite to the impact point is caused again by a surface layer detached due to the interference of the outgoing and incoming (reflected) tensile waves after impact. With increasing impact velocity the sample gets more and more shattered, hence, the first and the second peaks of the curves move in the opposite directions, while the detachment zones hardly change. This non-homogeneous spatial variation of cracking has the consequence that for the function $\langle m \rangle (x_0/L, v_0)$ no such scaling structure exists as Eq. (10) for the y_0 dependence.

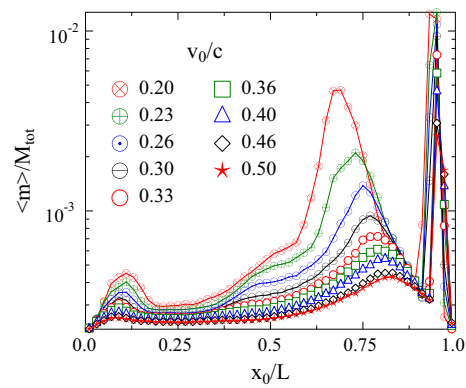


Fig. 9 (Color online) Average mass of fragments as a function of the x_0 coordinate of their center of mass position in the original body for the plate thickness $H = 3$. No scaling collapse can be achieved

At higher plate thicknesses H the x_0 dependence of the average fragment mass remains practically the same, while along the other two coordinate axes y_0 and z_0 the local maxima gradually diminish since the crack pattern loses its regularity with increasing H .

5.2 Spatial dependence of fragment velocities

In order to clarify how the spatial position of the fragments inside the original body determines their final state velocity, we calculated the average value of the velocity components of fragments as a function of their center of mass coordinates inside the original sample as it has been presented for the mass of fragments. Figure 10 presents the average of the absolute value of the y component of fragment velocities $\langle |v_y| \rangle$ as a function of y_0 for the lowest plate thickness $H = 3$ at several impact velocities. The zero linear momentum of the system in the y direction has the consequence that

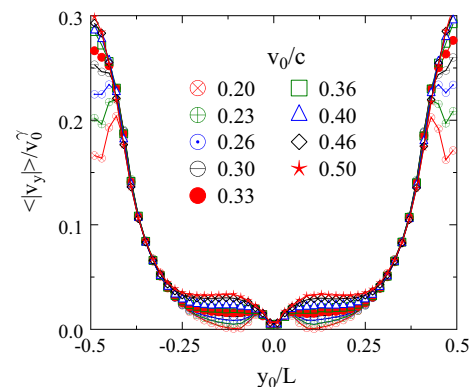


Fig. 10 (Color online) The absolute value of the velocity component v_y of fragments as a function of the center of mass position y_0 inside the original body for the plate thickness $H = 3$ at several impact velocities. The data is rescaled along the vertical axis with a power of the impact velocity. Best collapse is achieved with the exponent $\gamma = 0.8$

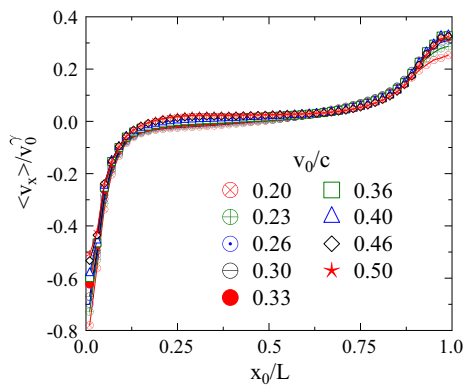


Fig. 11 (Color online) The velocity component v_x of fragments as a function of the center of mass position x_0 inside the original body for the same plate thickness and impact velocities as in Fig. 10. For the exponent $\gamma = 0.8$ was used to obtain best collapse

the corresponding velocity component $\langle |v_y| \rangle$ is a symmetric function with respect to the $y_0 = 0$ axis. It can be observed that fragments along the symmetry axis have zero velocity component $v_y = 0$, and $\langle |v_y| \rangle$ increases monotonically with the distance from the axis. Deviation from this generic trend occurs for the lowest impact velocities $v_0/c < 0.33$, where a local minimum is formed close to the symmetry axis and another one in the detachment zone close to the sample surface. In Fig. 10 the value of $\langle |v_y| \rangle$ is rescaled with a power γ of the impact velocity to obtain collapse of the curves belonging to different values of v_0 . The good quality data collapse shows the validity of the scaling form

$$\langle |v_y| \rangle (y_0/L, v_0) = v_0^\gamma \Phi(y_0/L), \quad (11)$$

where $\gamma = 0.8$ was used for the exponent in the figure. The scaling structure expresses that at a given location inside the body the velocity of fragments increases proportional to v_0^γ when changing the impact velocity. Note that the scaling function $\Phi(y_0/L)$ has no dependence on v_0 , it solely comprises the spatial dependence of the velocity components.

The momentum conservation implies the same overall behavior for the z component of the velocity of fragments as what we have presented for the y component.

For the x component of the fragment velocity we present the average $\langle v_x \rangle$ in Fig. 11 as a function of x_0 without taking the absolute value since no symmetry is expected. It can be observed that close to the sample surface $x_0/L \approx 0$ the value of $\langle v_x \rangle$ is negative which shows that the majority of fragments is back-scattered. Going inside the sample $\langle v_x \rangle$ is a monotonically increasing function of the position along the impact direction, however, about the middle of the sample the average velocity component remains close to zero for a relatively broad range of x_0 . The highest positive value of $\langle v_x \rangle$ is reached by the fragments which are detached from the sample surface opposite to the impact point, however,

the fastest fragments are the back-scattered powder particles at the impact site. Figure 11 also demonstrates that $\langle v_x \rangle$ has the same scaling structure Eq. (11) as the y component and even the same value of the exponent $\gamma = 0.8$ was used to achieve best collapse in the figure.

Increasing the plate thickness the overall behavior of the spatial distribution of the fragment velocities remains essentially the same, i.e. at all plate thicknesses the same scaling behavior Eq. (11) is recovered where even the exponent γ proved to have the same value irrespective of H . Only the precise shape of the scaling function Φ depends on the plate thickness.

6 Correlation of fragment mass and velocity

A large amount of experimental efforts have been devoted to investigate the velocity of fragments and its correlation with the fragment mass [21–24]. The mass-velocity correlation of fragments is usually characterized by evaluating the average value of the magnitude of the velocity $\langle v \rangle$ of fragments as a function of their mass m . In order to determine this quantity, in our calculations the fragment mass m was logarithmically binned and the arithmetic average of the velocity magnitude of fragments was calculated for each bin.

Figure 12 presents the $\langle v \rangle (m, v_0)$ function for the lowest plate thickness $H = 3$ considered at several impact velocities spanning both the damage $v_0 < v_c$ and fragmented $v_0 > v_c$ phases. Note that in the damage phase of the breakup process the curves have a gap where no fragments fall, while in the fragmented phase the gap disappears and a continuous curve is obtained. In the damage phase one or two dominating fragments are created comparable to the original mass of the body together with numerous smaller pieces. In Fig. 12 the remarkable result is that in the damage phase a strong mass-

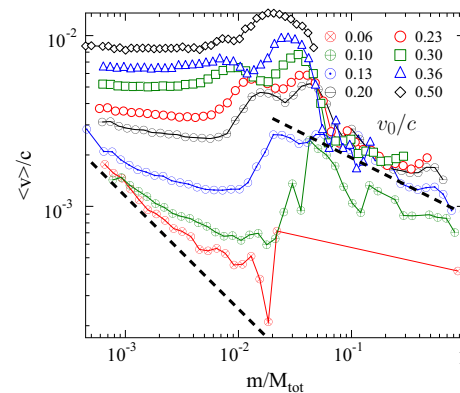


Fig. 12 (Color online) Average velocity of fragments $\langle v \rangle$ as a function of their mass m . Impact velocities v_0 are considered both in the damage and fragmented phases. The straight lines represent power laws with exponents $1/3$ and $1/6$ to guide the eye

velocity correlation of fragments emerges: for small pieces the velocity of fragments decreases with increasing mass. Lowering the impact velocity the functional form of $\langle v \rangle (m)$ tends to a power law

$$\langle v \rangle \sim m^{-\nu}, \quad (12)$$

where the exponent can be approximated as $\nu = 1/3$. Since at low impact velocities the number of fragments is limited, a large number of samples had to be generated to obtain reliable results. At the lowest value of v_0 the correlated regime extends to fragment masses $m/M_{tot} \approx 0.02$ followed by the mass-gap so that all small sized pieces have correlated mass and velocity. As v_0 increases the dominating fragments break up into smaller pieces and the mass-velocity correlation in the low mass regime gradually disappears, i.e. the $\langle v \rangle (m, v_0)$ curves become horizontal. At the same time, in the vicinity of the critical point v_c a new correlated regime develops for large fragment masses. The correlation is weaker in the sense that the exponent ν of the power law regime $\nu = 1/6$ is lower (see Fig. 12).

It can be seen in Fig. 12 that further increasing v_0 , in the fragmented regime the power law correlation gradually disappears so that the average velocity attains a constant value independent of the mass of fragments. Note that one or two humps develop on the curves in the mass range $0.008 < m/M_{tot} < 0.04$. These humps correspond to the fragments detached along the boundary of the sample. These pieces break off the body at an early stage of the breakup process and escape with a relatively high impact velocity.

Computer simulations revealed that the mass-velocity correlation of fragments prevails only for low plate thicknesses, i.e. for quasi two-dimensional bodies. Increasing H the correlation gradually disappears and for bulk samples no correlation could be pointed out. This is illustrated in Fig. 13

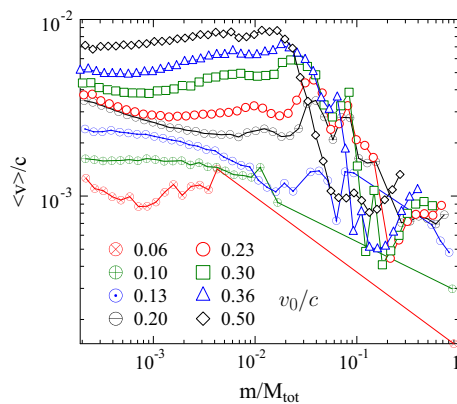


Fig. 13 (Color online) Analysis of the mass-velocity correlation for the highest plate thickness considered $H = 15$. No systematic dependence of the average fragment velocity on the fragment mass can be pointed out

for the thickness $H = 15$. Here even the detached pieces do not have a remarkable effect, their characteristic mass can not be identified in the figure.

7 Discussion

We presented a discrete element study of the fragmentation of plate-like brittle solids focusing on the velocity distribution and mass-velocity correlation of fragments. Simulations were performed by varying the impact velocity and the thickness of the plate which controlled the degree of breakup from damage to fragmentation and the geometry of the sample from thin plates to three-dimensional bulk solids, respectively. The initial condition we implemented well mimics the experimental setups where a projectile hits the sample surface but penetration is prevented, and the case when the explosion of a surface charge generates a shock wave in the solid. DEM has the advantage that all details of the model system can be very well controlled making it possible to reveal relations which may remain hidden in real experiments.

Based on the simulations we can deduce a simple physical picture about the process of impact induced breakup of heterogeneous solids: The formation of fragments and their final state mass and velocity are determined by the complex dynamics of elastic waves generated by the impact. As a consequence, large fragments are formed close to the middle of the sample making up a core, which gets shifted along the direction of impact with increasing impact velocity. The surrounding material of the core breaks up into a large number of small sized pieces and flies outward creating an expanding cloud of fragments. The results are in a good qualitative agreement with the experimental findings on impact induced breakup of heterogeneous materials [21–24].

We showed that the fastest fragments are the powder particles ejected in the vicinity of the impact point and the pieces created in the detachment zone opposite to the impact point. These fragments determine the cutoffs of the probability distributions of the velocity components of fragments. Due to momentum conservation the distributions of the velocity components perpendicular to the impact direction are symmetric functions with zero average. The standard deviation of the distributions increases linearly with the impact velocity and decreases as a sub-linear power law of the plate thickness. For the functional form of the distributions a power law asymptotics was found followed by an exponential cut-off. Along the impact direction the primary ejecta proved to have a unique distribution which can be approximated with a Gaussian. For the rest of the fragments the distribution has the same qualitative form as for the other two components with an additional asymmetry caused by the conservation of linear momentum.

In experiments, information on the velocity distribution of fragments is rather sparse since a large fraction of fragments cannot be captured. This limitation hinders the detailed comparison of our results to experimental findings. In 2D discrete element simulations of the fragmentation of disc-shape samples induced by impact against a hard wall, the distribution of both velocity components were found to be close to a Gaussian [7, 12], different from what we observed here. The possible explanation is the difference of the boundary conditions: due to the hard wall fragments spend a sufficient time confined to suffer collisions which can lead to a kind of thermalization before global expansion sets on. The free boundaries of our sample let the system freely expand resulting in a slower decay of the distributions.

It has been shown for vibrated granular beds that the probability distribution of the relative velocity of particles has different functional forms in the solid and fluidized phases [39]: in the solid phase where the particles are confined to the local vicinity of their stable position, the velocity distribution proved to be a Gaussian, while in the fluidized phase the higher mobility of particles leads to the emergence of a power law tail described by the t-distribution [39, 40]. The particle motion in the two phases is very similar to the situation of fragments in 2D and 3D fragmentation processes outlined above so that the same mechanism can be responsible for the emergence of power law and Gaussian velocity distributions of fragments as for granular matter. The functional form Eq. (8) deduced for the velocity distribution of fragments is consistent with the t-distribution [41], although the direct application of the t-distribution gives a somewhat lower quality fit than our expression.

The most important outcome of the present work is the relation of the mass and velocity of fragments: simulations give a strong evidence that correlation can emerge between the mass and velocity of fragments, however, the presence and absence of the correlation depend both on the impact velocity and on the geometry of the sample. Correlation is only found for quasi 2D thin plates embedded in the 3D space, when increasing the plate thickness to 3D bulk samples no systematic correlation could be pointed out. For thin plates the mass-velocity correlation emerges for small fragment masses in the damage phase, i.e. at sufficiently low impact velocity the average velocity of fragments decreases as a power law of their mass. At higher impact velocities the correlation disappears in the low mass regime, however, in the vicinity of the critical point of fragmentation a power law correlation emerges again for the largest fragments but with a lower exponent. Due to technical constraints, experimental studies on the mass-velocity correlation typically focus on the larger fragments of the fragmented phase of breakup. It is interesting to note that the corresponding value of the power law exponent $1/6$ we obtained falls in the range of experimental results [22]. The absence of correlation well above

the critical point is also in agreement with experiments [24]. Further laboratory experiments are needed to check the emergence of correlations in the damage phase of breakup, where difficulties arise because of the small fragment size and low fragment number.

Computer simulations revealed that the position of fragments inside the original body with respect to the impact site and to the core determine the velocity and mass of fragments: the velocity increases with the distance from the core, while the fragment mass is sensitive to the details of the stress field resulting in a complex mass pattern in the body. As a very interesting novel result we deduced a scaling form of the spatial distribution of the velocity components obtained at different impact velocities. The scaling implies that the velocity components of fragments created at any location inside the body increase with a power of the impact velocity. The positional dependence is comprised in a scaling function which does not depend on the impact velocity. For fragment masses a similar scaling form could be obtained solely perpendicular to the impact direction, however, along the impact a more complex non-homogeneous dependence on the impact velocity was revealed. Our simulation results suggest that the origin of the mass-velocity correlation is that the mass and velocity of fragments get connected through their positional dependence inside the body.

Acknowledgments This research was supported by the European Union and the State of Hungary, co-financed by the European Social Fund in the framework of the Projects TAMOP-4.2.2.A-11/1/KONV-2012-0036 and TAMOP-4.2.4.A/2-11/1-2012-0001 National Excellence Program. We also acknowledge the support of OTKA K84157.

References

- Herrmann, H.J., Roux, S. (eds.): *Statistical Models for the Fracture of Disordered Media*. Random Materials and Processes. Elsevier, Amsterdam (1990)
- Aström, J.A.: Statistical models of brittle fragmentation. *Adv. Phys.* **55**, 247–278 (2006)
- Aström, J.A., Vallot, D., Schäfer, M., Welty, E.Z., O'Neil, S., Bartholomäus, T.C., Liu, Y., Riikilä, T.I., Zwinger, T., Timonen, J., Moore, J.C.: Termini of calving glaciers as self-organized critical systems. *Nat. Geosci.* **7**(12), 874–878 (2014)
- Turcotte, D.L.: *Fractals and Chaos in Geology and Geophysics*. Cambridge University Press, Cambridge (1997)
- Botke, W.F., Cellino Jr., A., Paolicchi, P., Binzel, R.P.: *Asteroids III*. University of Arizona Press, Tucson (2002)
- Kun, F., Herrmann, H.J.: A study of fragmentation processes using a discrete element method. *Comput. Methods Appl. Mech. Eng.* **138**, 3–18 (1996)
- Kun, F., Herrmann, H.J.: Fragmentation of colliding discs. *Int. J. Mod. Phys. C* **7**, 837–855 (1996)
- Aström, J., Holian, A., Timonen, J.: Universality in fragmentation. *Phys. Rev. Lett.* **84**, 3061–3064 (2000)
- Aström, J.A., Ouchterlony, F., Linna, R.P., Timonen, J.: Universal dynamic fragmentation in D dimensions. *Phys. Rev. Lett.* **92**, 245506 (2004)

10. Wittel, F.K., Kun, F., Herrmann, H.J., Kröplin, B.H.: Fragmentation of shells. *Phys. Rev. Lett.* **93**, 035504 (2004)
11. Wittel, F.K., Kun, F., Herrmann, H.J., Kröplin, B.H.: Study on the fragmentation of shells. *Int. J. Fract.* **140**, 243–255 (2006)
12. Behera, B., Kun, F., McNamara, S., Herrmann, H.J.: Fragmentation of a circular disc by impact on a frictionless plate. *J. Phys. Condens. Matter* **17**, 2439 (2005)
13. Timár, G., Blömer, J., Kun, F., Herrmann, H.J.: New universality class for the fragmentation of plastic materials. *Phys. Rev. Lett.* **104**, 095502 (2010)
14. Timár, G., Kun, F., Carmona, H.A., Herrmann, H.J.: Scaling laws for impact fragmentation of spherical solids. *Phys. Rev. E* **86**, 016113 (2012)
15. Pál, G., Varga, I., Kun, F.: Emergence of energy dependence in the fragmentation of heterogeneous materials. *Phys. Rev. E* **90**, 062811 (2014)
16. Kun, F., Wittel, F.K., Herrmann, H.J., Kröplin, B.H., Maloy, K.J.: Scaling behaviour of fragment shapes. *Phys. Rev. Lett.* **96**, 025504 (2006)
17. Domokos, G., Kun, F., Sipos, A.A., Szabó, T.: Universality of fragment shapes. *Sci Rep* **5**, 9147–9154 (2015)
18. Michikami, T., Hagermann, A., Kadokawa, T., Yoshida, A., Shimada, A., Hasegawa, S., Tsuchiyama, A.: Fragment shapes in impact experiments ranging from cratering to catastrophic disruption. *Icarus* **264**, 316–330 (2016)
19. Blasio, F.V.: Rheology of a wet, fragmenting granular flow and the riddle of the anomalous friction of large rock avalanches. *Granul. Matter* **11**, 179–184 (2009)
20. Imre, B., Laue, J., Springman, S.M.: Fractal fragmentation of rocks within sturzstroms: insight derived from physical experiments within the ETH geotechnical drum centrifuge. *Granul. Matter* **12**, 267–285 (2010)
21. Fujiwara, A., Tsukamoto, A.: Experimental study on the velocity of fragments in collisional breakup. *Icarus* **44**, 142–153 (1980)
22. Nakamura, A., Sugiyama, K., Fujiwara, A.: Velocity and spin of fragments from impact disruptions: I. An experimental approach to a general law between mass and velocity. *Icarus* **100**(1), 127–135 (1992)
23. Onose, N., Fujiwara, A.: Massvelocity distributions of fragments in oblique impact cratering on gypsum. *Meteorit. Planet. Sci.* **39**(2), 321–331 (2004)
24. Kadono, T., Arakawa, M., Mitani, N.: Fragment velocity distribution in the impact disruption of thin glass plates. *Phys. Rev. E* **72**, 045106(R) (2005)
25. Giblin, I.: New data on the velocity-mass relation in catastrophic disruption. *Planet. Space Sci.* **46**(8), 921–928 (1998)
26. Kun, F., Varga, I., Lennartz-Sassinek, S., Main, I.G.: Approach to failure in porous granular materials under compression. *Phys. Rev. E* **88**, 062207 (2013)
27. Kun, F., Varga, I., Lennartz-Sassinek, S., Main, I.G.: Rupture cascades in a discrete element model of a porous sedimentary rock. *Phys. Rev. Lett.* **112**, 065501 (2014)
28. Pöschel, T., Schwager, T.: *Computational Granular Dynamics*. Springer, Berlin (2005)
29. Addetta, G.A.D., Kun, F., Ramm, E., Herrmann, H.J.: In: Vermeer, P.A., et al. (eds.) *Continuous and Discontinuous Modelling of Cohesive-Frictional Materials*. Lecture Notes in Physics. Springer, Berlin; Heidelberg; New York (2001)
30. D’Addetta, G.A., Kun, F., Ramm, E.: On the application of a discrete model to the fracture process of cohesive granular materials. *Granul. Matter* **4**, 77–90 (2002)
31. Carmona, H.A., Wittel, F.K., Kun, F., Herrmann, H.J.: Fragmentation processes in impact of spheres. *Phys. Rev. E* **77**, 051302 (2008)
32. Kadono, T.: Fragment mass distribution of platelike objects. *Phys. Rev. Lett.* **78**, 1444–1447 (1997)
33. Kadono, T., Arakawa, M.: Crack propagation in thin glass plates caused by high velocity impact. *Phys. Rev. E* **65**, 035107 (2002)
34. Giblin, I., Martelli, G., Smith, P., Martino, M.D.: Simulation of hypervelocity impacts using a contact charge. *Planet. Space Sci.* **42**(12), 1027–1030 (1994)
35. Kun, F., Herrmann, H.J.: Transition from damage to fragmentation in collision of solids. *Phys. Rev. E* **59**, 2623–2632 (1999)
36. Katsuragi, H., Sugino, D., Honjo, H.: Crossover of weighted mean fragment mass scaling in two-dimensional brittle fragmentation. *Phys. Rev. E* **70**, 065103(R) (2004)
37. Katsuragi, H., Sugino, D., Honjo, H.: Scaling of impact fragmentation near the critical point. *Phys. Rev. E* **68**, 046105 (2003)
38. Katsuragi, H., Ihara, S., Honjo, H.: Explosive fragmentation of a thin ceramic tube using pulsed power. *Phys. Rev. Lett.* **95**, 095503 (2005)
39. Taguchi, Y.-H., Takayasu, H.: Power law velocity fluctuations due to inelastic collisions in numerically simulated vibrated bed of powder. *Europhys. Lett.* **30**, 499–504 (1995)
40. Jaeger, H.M., Nagel, S.R., Behringer, R.P.: Granular solids, liquids, and gases. *Rev. Mod. Phys.* **68**, 1259–1273 (1996)
41. Grigelionis, B.: *Student t-Distribution and Related Stochastic Processes*. Springer, Berlin (2013)